



Published in final edited form as:

*Nano Res.* 2018 October ; 11(10): 5596–5603. doi:10.1007/s12274-018-2082-0.

## Co-delivery of mRNA and SPIONs through amino-ester nanomaterials

Xiao Luo<sup>1</sup>, Weiyu Zhao<sup>1</sup>, Bin Li<sup>1</sup>, Xinfu Zhang<sup>1</sup>, Chengxiang Zhang<sup>1</sup>, Anna Bratasz<sup>2</sup>, Binbin Deng<sup>3</sup>, David W. McComb<sup>3</sup>, Yizhou Dong<sup>1,4,5,6,7,8</sup>

<sup>1</sup>Division of Pharmaceutics and Pharmaceutical Chemistry, College of Pharmacy, The Ohio State University, Columbus, Ohio 43210, USA

<sup>2</sup>Small Animal Imaging Core, The Ohio State University, Columbus, Ohio 43210, USA

<sup>3</sup>Center for Electron Microscopy and Analysis, Department of Materials Science and Engineering, The Ohio State University, Columbus, Ohio 43210, USA

<sup>4</sup>Department of Biomedical Engineering, The Ohio State University, Columbus, Ohio 43210, USA

<sup>5</sup>The Center for Clinical and Translational Science, The Ohio State University, Columbus, Ohio 43210, USA

<sup>6</sup>The Comprehensive Cancer Center, The Ohio State University, Columbus, Ohio 43210, USA

<sup>7</sup>Dorothy M. Davis Heart & Lung Research Institute, The Ohio State University, Columbus, Ohio 43210, USA

<sup>8</sup>Department of Radiation Oncology, The Ohio State University, Columbus, Ohio 43210, USA

### Abstract

Nanoparticles have been widely explored for combined therapeutic and diagnostic applications. For example, lipid-based nanoparticles have been used to encapsulate multiple types of agents and achieve multi-functions. Herein, we enabled a co-delivery of mRNA molecules and superparamagnetic iron oxide nanoparticles (SPIONs) by using an amino-ester lipid-like nanomaterial. An orthogonal experimental design was used to identify the optimal formulation. The optimal formulation, MPA-Ab-8 LLNs, not only showed high encapsulation of both mRNA and SPIONs, but also increased the  $r_2$  relaxivity of SPIONs by more than 1.5-fold *in vitro*. MPA-Ab-8 LLNs effectively delivered mRNA and SPIONs into cells, and consequently induced high protein expression as well as strong MRI contrast. Consistent herewith, we observed both mRNA-mediated protein expression and an evident negative contrast enhancement of MRI signal in mice. In conclusion, amino-ester nanomaterials demonstrate great potential as delivery vehicles for theranostic applications.

---

Correspondence to: Yizhou Dong.

Address correspondence to dong.525@osu.edu.

**Electronic Supplementary Material:** Supplementary material (formulation table, orthogonal design, chemical structures, characterization of MPA-Ab-SPIONs LLNs, and T2 relaxation time quantification of mouse spleen) is available in the online version of this article at <https://doi.org/10.1007/s12274-018-2082-0>.

## Keywords

amino-ester nanomaterials; lipid-like nanoparticles (LLNs); dual-functional; superparamagnetic iron oxide nanoparticles (SPIONs); mRNA delivery; magnetic resonance imaging (MRI)

---

## 1 Introduction

In recent years, many efforts have been made to explore efficient chemical compositions and formulation methods for establishing effective platforms for mRNA delivery [1, 2]. Many of these delivery systems demonstrated the concept of mRNA-based therapeutics for expression of functional proteins, such as erythropoietin, factor IX and Cas9 [3–10]. Lipid and lipid-like nanoparticles (LNPs and LLNs) are representative delivery systems for efficient delivery of RNAs [11–15]. Previously, we developed a series of lipid-like nanomaterials for mRNA delivery and improved their delivery efficiency by utilizing an orthogonal experimental design to fine-tune the molar ratio of formulation components [16–19]. Among these nanomaterials, amino-ester nanomaterials allowed efficient delivery of Cas9 mRNA and gene editing in a mouse model [19]. Meanwhile, these amino-ester nanomaterials also exhibited tunable biodegradability since they were decorated with different ester groups. Because of these favorable properties, amino-ester nanomaterials merit further development for therapeutic and diagnostic applications.

Superparamagnetic iron oxide nanoparticles (SPIONs) are superparamagnetic contrast agents, which generate negative contrast enhancement in a T2-weighted image [20, 21]. SPIONs, with high transverse relaxivity ( $r_2$ ), are compatible with live imaging *in vivo* [22]. After administration, SPIONs are capable of shortening the T2 relaxation time of surrounding water protons and generate dark signals (negative contrast) [23]. Among the different types of magnetic resonance imaging (MRI) contrast agents, SPIONs are biocompatible and biodegradable [24]. However, SPIONs have limited cell membrane permeability [25]. To address this issue, lipid nanoparticles have been employed to enable the delivery of SPIONs into cells [26–28]. Based on previous findings, we hypothesized that amino-ester nanomaterials may be capable of simultaneous delivery of mRNA and SPIONs. Therefore, in this study, we investigated formulations using amino-ester nanomaterials to co-deliver mRNA and SPIONs. These nanoparticles possess dual functions that may potentially enable real-time and non-invasive visualization of diseased sites and the production of efficacious proteins for therapeutic applications in future.

## 2 Experimental

### 2.1 Materials

mRNAs encoding enhanced green fluorescent protein (eGFP) and firefly luciferase (FLuc) were purchased from TriLink Biotechnologies, Inc. (San Diego, CA, USA). 1,2-Dioleoyl-sn-glycero-3-phosphoethanolamine (DOPE) was purchased from Avanti Polar Lipids, Inc. (Alabaster, AL, USA). 1,2-Dimyristoyl-sn-glycerol, methoxypolyethylene glycol (DMG-PEG<sub>2000</sub>) was purchased from NOF America Corporation (White Plains, NY, USA).

SPIONs were purchased from AC Diagnostic, Inc. (Fayetteville, AR, USA). Cholesterol (Chol) was purchased from Sigma-Aldrich (St. Louis, MO, USA).

## 2.2 Formulation of mRNA-SPION LLNs

MPA-Ab or TT3 (Fig. S1 in the Electronic Supplementary Material (ESM)) was formulated into nanoparticles with DOPE, Chol, DMG-PEG<sub>2000</sub>, SPIONs, and mRNA. Briefly, MPA-Ab or TT3 was mixed with DOPE, Chol, and DMG-PEG<sub>2000</sub> in ethanol at a previously identified optimal molar ratio of 20:30:40:0.75 [16]. mRNA and a various amount of SPIONs (0, 5, 10, or 20 µg) were mixed and further diluted in 10 mM citric acid buffer to prepare the aqueous phase. Subsequently, equal volumes of the ethanol and aqueous phases were mixed and then diluted with PBS (1:1, v/v) to prepare the desired nanomaterials.

## 2.3 mRNA-SPION LLN-mediated eGFP expression assay

The human hepatocellular carcinoma cell line Hep3B was purchased from American Type Culture Collection (Manassas, VA, USA) and was cultured in Eagle's Minimum Essential Medium supplemented with 10% fetal bovine serum. Cells were seeded in 6-well plates at a density of  $2 \times 10^5$  cells/well. Twenty-four hours later, 15 µL of eGFP mRNA-SPION LLNs (150 ng mRNA equivalent) was added to the cells. After 24 h of treatment, the cells were trypsinized, washed, and collected. Green fluorescence intensity was quantified with a BD LSR II flow cytometer (San Jose, CA, USA).

## 2.4 Orthogonal experimental design

The optimal formulation (molar ratio) for MPA-Ab LLNs was determined through an orthogonal experiment. Each formulation component (MPA-Ab, DOPE, Chol, DMG-PEG<sub>2000</sub>, and SPIONs) was assigned four levels, and a total of 16 combinations were evaluated. The optimal formulation molar ratio was identified using a data analysis method reported previously [16].

## 2.5 Characterization of mRNA-SPION LLNs

Thirty microliters of mRNA-SPION LLNs was diluted in Milli-Q water. Then, the particle size and surface charge of mRNA-SPION LLNs were determined using a NanoZS Zetasizer (Malvern, Worcestershire, UK). Formulation MPA-Ab-8 was stored at 4 °C and its particle size was measured at day 1 and day 7 to test stability. Quant-iT™ RiboGreen RNA Assay Kit was used following the manufacturer's protocol to quantify the mRNA encapsulation efficiency.

## 2.6 Cryo-transmission electron microscopy (cryoTEM)

A small volume of MPA-Ab-8 LLNs (3 µL) was loaded onto a 400-mesh carbon-coated grid. The grid was immediately submerged into liquid ethane after extra liquid was blotted away. After a thin film of amorphous ice was formed, the grid was transferred to a Gatan 626 cryotransfer holder (Gatan, Pleasanton, CA, USA) while being kept at -196 °C in liquid nitrogen. The cryotransfer holder was subsequently loaded onto a Tecnai F20 S/TEM (Thermo-Fisher Scientific, Hillsboro, OR, USA) for image acquisition. Images were recorded at 200 kV with a nominal magnification of 80,000× under low-dose conditions.

## 2.7 Phantom MRI study

Standard SPION solutions were prepared by serial dilutions from a starting  $\text{Fe}_3\text{O}_4$  concentration of 0.4 mM. Formulation MPA-Ab-8 was diluted to a  $\text{Fe}_3\text{O}_4$  concentration of 0.4 mM and further serially diluted 1:2 four times. A total of 12 vials (PBS, MPA-Ab-8 LLNs without SPIONs, 5 gradients of standards and 5 gradients of MPA-Ab-8 LLNs) were measured using a BioSpec 94/30 Imaging System (Bruker Co., Billerica, MA, USA).  $T_2$  mapping was performed following a multi-slice multi-echo protocol: echo time (TE) = 15 ms, number of echoes = 36, repetition time (TR) = 4,000 ms, number of averages (NA) = 1, field of view (FOV) = 3 cm  $\times$  3 cm, matrix = 256  $\times$  256, 2 mm slice thickness.

## 2.8 Cell-pellet MRI

MPA-Ab-8 LLNs and MPA-Ab-8 (without SPIONs) LLNs were formulated and dialyzed in PBS using 3.5 K MWCO Slide-A-Lyzer™ Dialysis Cassettes (Thermo Fisher Scientific, Waltham, MA, USA) one day before usage and were stored at 4 °C. Hep3B cells were cultured at 37 °C in a 5% carbon dioxide incubator to 90% confluency. Formulation MPA-Ab-8 was added to the cells at a final  $\text{Fe}_3\text{O}_4$  concentration of 0.003 or 0.015 mM. MPA-Ab-8 (without SPIONs) LLNs were used as a control. After 3 h of incubation, the cells were washed, trypsinized, centrifuged, and collected for MRI.  $T_2$ -weighted images were acquired using a rapid acquisition with relaxation enhancement (RARE) protocol: TE = 12 ms, TR = 3,500 ms, rare factor = 8, NA = 1, FOV = 3 cm  $\times$  3 cm, matrix = 256  $\times$  256, 1 mm slice thickness.  $T_2$  mapping was performed following a multi-slice multi-echo protocol: TE = 9.8 ms, number of echoes = 36, TR = 4,000 ms, NA = 1, FOV = 3 cm  $\times$  3 cm, matrix = 256  $\times$  256, 2 mm slice thickness.

## 2.9 Biodistribution study

All procedures used in animal studies were approved by the Institutional Animal Care and Use Committee (IACUC) at The Ohio State University and were consistent with local, state, and federal regulations as applicable. FLuc mRNA-encapsulated MPA-Ab-8 LLNs were intravenously injected into an 8-week-old C57BL/6 mouse through the tail vein at an mRNA dose of 0.5 mg/kg. An untreated mouse served as a control. After 6 h of treatment, 150  $\mu\text{L}$  of 30  $\text{mg}\cdot\text{mL}^{-1}$  D-luciferin was administered intraperitoneally. Eight minutes later, the mice were euthanized to collect heart, liver, spleen, lung, and kidneys. Bioluminescence radiance was quantified using an IVIS Lumina II imaging system (PerkinElmer, Inc., Waltham, MA, USA).

## 2.10 *In-vivo* MRI assay

An 8-week-old C57BL/6 mouse was anaesthetized, cannulated at the tail vein, and carefully transferred into the MRI scanner (BioSpec 94/30 Imaging System).  $T_2$ -weighted images of spleen were acquired as no-treatment control. Formulation MPA-Ab-8 was then administered at a  $\text{Fe}_3\text{O}_4$  dose of 1.6  $\text{mg}\cdot\text{kg}^{-1}$  and  $T_2$ -weighted images of spleen were captured immediately after administration.  $T_2$ -weighted images were collected using the following parameters: RARE protocol, TE = 12.75 ms, TR = 3,723.8 ms, rare factor = 8, NA = 4, FOV = 2.8 cm  $\times$  2.8 cm, matrix = 286  $\times$  286, 1 mm slice thickness, 30 slices. Agarose (1%) was used as a standard for signal intensity normalization.

### 3 Results and discussion

MPA-Ab (Fig. S1 in the ESM) is a representative example of biodegradable amino-ester LLNs that allows effective mRNA delivery according to our prior study [19]. In order to incorporate multiple functions in MPA-Ab LLNs, we encapsulated both SPIONs and mRNA. Formulation ratios are listed in Table S1 in the ESM. We evaluated these formulations in Hep3B cells and compared them with TT3 LLNs, a previously reported material (Fig. S1 in the ESM), as a positive control [16]. Through flow-cytometric analysis, we found that MPA-Ab LLNs displayed higher delivery efficiency of eGFP mRNA than TT3 LLNs with the same amount of SPIONs (0, 5, 10, or 20  $\mu\text{g}$ ) (Fig. 1).

Moreover, the formulation MPA-Ab-S1 (addition of 5  $\mu\text{g}$  SPIONs in the MPA-Ab LLNs) slightly improved mRNA delivery efficiency compared to MPA-Ab LLNs without SPIONs. In order to identify an optimal formulation of mRNA and SPION co-encapsulated MPA-Ab LLNs, we performed an orthogonal experiment. We assigned four levels to each formulation component (MPA-Ab, DOPE, Chol, DMG-PEG<sub>2000</sub>, and SPIONs) and then investigated their effects on mRNA delivery efficiency (Table S2 in the ESM). As shown in Fig. 2(a), the eGFP mRNA delivery efficiency of MPA-Ab-8 LLNs was the highest among all the formulations, and it was approximately 2.5-fold higher than that of the original formulation MPA-Ab LLNs. Figures 2(b), 2(d), and 2(e) show that formulation components MPA-Ab, Chol, and DMG-PEG<sub>2000</sub> reached their highest delivery efficiency at molar ratios of 25, 45, and 0.75, respectively. DOPE at a molar ratio of 60 reached the plateau (Fig. 2(c)) and 5  $\mu\text{g}$  of SPIONs was optimal for mRNA delivery (Fig. 2(f)). Therefore, the optimal formulation identified based on the trend analysis had a molar ratio of MPA-Ab/DOPE/Chol/PEG = 25/60/45/0.75 and an mRNA/SPIONs weight ratio of 1/2.5, that is the formulation MPA-Ab-8 in the orthogonal table. We also characterized the physicochemical properties of the formulations in the orthogonal table, including particle size, zeta potential, and mRNA encapsulation efficiency. The correlation of green fluorescence intensity with these three parameters was analyzed (Fig. S2 in the ESM). The results showed that both particle size and zeta potential exhibited a significant positive correlation with green fluorescence intensity. No correlation was observed between green fluorescence intensity and mRNA encapsulation efficiency.

The features of SPIONs encapsulated in MPA-Ab-8 LLNs were studied. We first measured the size distribution of free SPIONs and MPA-Ab-8 LLNs, separately. Mean particle sizes were approximately 3 and 70 nm for free SPIONs and MPA-Ab-8 LLNs, respectively (Figs. 3(a) and 3(b)). No typical size distribution pattern of SPIONs was detected for MPA-Ab-8 LLNs, suggesting that SPIONs were well encapsulated into the MPA-Ab-8 LLNs. In addition, MPA-Ab-8 LLNs were stable for at least one week when stored at 4 °C (Fig. 3(c) and Fig. S3 in the ESM). The particle size and morphology of MPA-Ab-8 LLNs was further determined by cryoTEM. As shown in Fig. 3(d), the particles had a nearly spherical shape and their sizes were consistent with dynamic light scattering (DLS) measurement results.

We then studied the usability of MPA-Ab-8 LLNs for *in-vitro* MR imaging. First, we performed a phantom MRI assay to investigate the effects of LLNs on transverse relativity ( $T_2$ ) of SPIONs [29]. Free SPIONs were used to prepare standards with five different Fe<sub>3</sub>O<sub>4</sub>

concentrations. Formulation MPA-Ab-8 was diluted to the same  $\text{Fe}_3\text{O}_4$  concentrations as the standards.  $T_2$  relaxation time for these samples was determined using a 9.4T MRI system. Transverse relaxivity was calculated using the following equation:  $r_2[\text{Fe}_3\text{O}_4] = 1/T_{2,x} - 1/T_0$  ( $T_{2,x}$  and  $T_0$  are  $T_2$  relaxation times of standards and PBS, or samples and no-SPIONs control) [29–31]. As shown in Figs. 4(a) and 4(b),  $r_2$  was determined to be  $4.238 \text{ mM}^{-1}\cdot\text{s}^{-1}$  for free SPIONs and  $6.502 \text{ mM}^{-1}\cdot\text{s}^{-1}$  for MPA-Ab-8 LLNs, respectively. The transverse relaxivity increased approximately 1.5-fold after the encapsulation, indicating that MPA-Ab-8 LLNs enhanced the contrast potential of SPIONs. Subsequently, we conducted a cell-pellet MRI study. Hep3B cells were treated with PBS, MPA-Ab-8 LLNs (without SPIONs), and MPA-Ab-8 LLNs at two concentrations (final  $[\text{Fe}_3\text{O}_4] = 0.003 \text{ mM}$  and  $0.015 \text{ mM}$ ).  $T_2$ -weighted images were acquired using the same system (Fig. 4(c)). The PBS-treated group appeared bright on  $T_2$ -weighted images, while increasing the amount of iron oxide was related to significant negative signal enhancement. Next, we performed  $T_2$  mapping for quantification (Fig. 4(d)). Cell pellets treated with  $0.003$  and  $0.015 \text{ mM}$  equivalent of iron oxide showed 90% and 44% relative  $T_2$  relaxation time compared to control MPA-Ab-8 (without SPIONs)-treated cell pellets. Results from *in-vitro* studies demonstrated that MPA-Ab-8 LLNs are capable of simultaneously delivering both mRNA molecules and MRI contrast agent SPIONs.

Given the promising *in-vitro* results, we next investigated the potential of MPA-Ab-8 LLNs for *in-vivo* applications. To study the mRNA delivery efficiency of MPA-Ab-8 LLNs *in vivo*, FLuc mRNA-encapsulated MPA-Ab-8 LLNs were administered to a mouse intravenously at an mRNA dose of  $0.5 \text{ mg/kg}$ . As shown in Fig. 5(a), the MPA-Ab-8 FLuc LLN-treated mouse displayed strong luminescence signal at both the liver and the spleen, while no signal was detected in the non-treated control mouse. Next, we investigated whether the MPA-Ab-8 LLNs were able to induce a negative contrast enhancement *in vivo*. In this experiment, formulation MPA-Ab-8 was intravenously injected into a mouse via the tail vein at a  $\text{Fe}_3\text{O}_4$  dose of  $1.6 \text{ mg/kg}$ . Compared to the non-treated condition, there was a dramatic decrease in  $T_2$  signal intensity at the spleen after administration (Fig. 5(b)), which reduced the signal by 49% (Fig. S4 in the ESM). Based on the above results, formulation MPA-Ab-8 demonstrated its dual functions *in vivo*: delivering mRNA and achieving non-invasive MR imaging.

## 4 Conclusions

In summary, we optimized amino-ester lipid-based nanoparticles for simultaneous delivery of mRNA and SPIONs. MPA-Ab LLNs showed a significantly higher mRNA delivery efficiency in Hep3B cells than did TT3 LLNs. Using an orthogonal experiment, the optimal formulation MPA-Ab-8 was identified, with an approximately 2.5-fold increase in mRNA delivery efficiency in comparison to the original formulation. MPA-Ab-8 LLNs displayed great potential for delivering functional mRNA and producing MRI contrast signals *in vivo*. Overall, the dual-functional nanoparticles provide a useful tool for future theranostic applications.

## Supplementary Material

Refer to Web version on PubMed Central for supplementary material.

## Acknowledgements

Y. D. acknowledges support from Early Career Investigator Award from the Bayer Hemophilia Awards Program, Research Awards from the National PKU Alliance, New Investigator Grant from the American Association of Pharmaceutical Scientists (AAPS) Foundation, Maximizing Investigators' Research Award 1R35GM119679 from the National Institute of General Medical Sciences as well as the start-up fund from the College of Pharmacy at The Ohio State University.

## References

- [1]. Islam MA; Reesor EKG; Xu YJ; Zope HR; Zetter BR; Shi JJ Biomaterials for mRNA delivery. *Biomater. Sci* 2015, 3, 1519–1533. [PubMed: 26280625]
- [2]. Hajj KA; Whitehead KA Tools for translation: Non-viral materials for therapeutic mRNA delivery. *Nat. Rev. Mater* 2017, 2, 17056.
- [3]. DeRosa F; Guild B; Karve S; Smith L; Love K; Dorkin JR; Kauffman KJ; Zhang J; Yahalom B; Anderson DG et al. Therapeutic efficacy in a hemophilia B model using a biosynthetic mRNA liver depot system. *Gene Ther* 2016, 23, 699–707. [PubMed: 27356951]
- [4]. Ramaswamy S; Tonnu N; Tachikawa K; Limphong P; Vega JB; Karmali PP; Chivukula P; Verma IM Systemic delivery of factor IX messenger RNA for protein replacement therapy. *Proc. Natl. Acad. Sci. USA* 2017, 114, E1941–E1950. [PubMed: 28202722]
- [5]. Kauffman KJ; Dorkin JR; Yang JH; Heartlein MW; DeRosa F; Mir FF; Fenton OS; Anderson DG Optimization of lipid nanoparticle formulations for mRNA delivery in vivo with fractional factorial and definitive screening designs. *Nano Lett* 2015, 15, 7300–7306. [PubMed: 26469188]
- [6]. Thess A; Grund S; Mui BL; Hope MJ; Baumhof P; Fotin-Mleczek M; Schlake T Sequence-engineered mRNA without chemical nucleoside modifications enables an effective protein therapy in large animals. *Mol. Ther* 2015, 23, 1456–1464. [PubMed: 26050989]
- [7]. Fenton OS; Kauffman KJ; McClellan RL; Appel EA; Dorkin JR; Tibbitt MW; Heartlein MW; DeRosa F; Langer R; Anderson DG Bioinspired alkenyl amino alcohol ionizable lipid materials for highly potent in vivo mRNA delivery. *Adv. Mater* 2016, 28, 2939–2943. [PubMed: 26889757]
- [8]. Yin H; Song CQ; Dorkin JR; Zhu LJ; Li YX; Wu QQ; Park A; Yang J; Suresh S; Bizhanova A et al. Therapeutic genome editing by combined viral and non-viral delivery of CRISPR system components *in vivo*. *Nat. Biotechnol* 2016, 34, 328–333. [PubMed: 26829318]
- [9]. Miller JB; Zhang SY; Kos P; Xiong H; Zhou KJ; Perelman SS; Zhu H; Siegwart DJ Non-viral CRISPR/ cas gene editing in vitro and in vivo enabled by synthetic nanoparticle co-delivery of Cas9 mRNA and sgRNA. *Angew. Chem., Int. Ed* 2017, 56, 1059–1063.
- [10]. Jiang C; Mei M; Li B; Zhu XR; Zu WH; Tian YJ; Wang QN; Guo Y; Dong YZ; Tan X A non-viral CRISPR/Cas9 delivery system for therapeutically targeting HBV DNA and *pcsk9 in vivo*. *Cell Res* 2017, 27, 440–443. [PubMed: 28117345]
- [11]. Cullis PR; Hope MJ Lipid nanoparticle systems for enabling gene therapies. *Mol. Ther* 2017, 25, 1467–1475. [PubMed: 28412170]
- [12]. Xue HY; Guo PB; Wen WC; Wong HL Lipid-based nanocarriers for RNA delivery. *Curr. Pharm. Des* 2015, 21, 3140–3147. [PubMed: 26027572]
- [13]. Zhao Y; Huang L Lipid nanoparticles for gene delivery. *Adv. Genet* 2014, 88, 13–36. [PubMed: 25409602]
- [14]. Leung AKK; Tam YYC; Cullis PR Lipid nanoparticles for short interfering RNA delivery. *Adv. Genet* 2014, 88, 71–110. [PubMed: 25409604]
- [15]. Kanasty R; Dorkin JR; Vegas A; Anderson D Delivery materials for siRNA therapeutics. *Nat. Mater* 2013, 12, 967–977. [PubMed: 24150415]
- [16]. Li B; Luo X; Deng BB; Wang JF; McComb DW; Shi YM; Gaensler KML; Tan X; Dunn AL; Kerlin BA et al. An orthogonal array optimization of lipid-like nanoparticles for mRNA delivery *in vivo*. *Nano Lett* 2015, 15, 8099–8107. [PubMed: 26529392]

- [17]. Li B; Luo X; Deng BB; Giancola JB; McComb DW; Schmittgen TD; Dong YZ Effects of local structural transformation of lipid-like compounds on delivery of messenger RNA. *Sci. Rep* 2016, 6, 22137. [PubMed: 26916931]
- [18]. Luo X; Li B; Zhang X; Zhao W; Bratasz A; Deng B; McComb DW; Dong Y Dual-functional lipid-like nanoparticles for delivery of mRNA and MRI contrast agents. *Nanoscale* 2017, 9, 1575–1579. [PubMed: 28067926]
- [19]. Zhang XF; Li B; Luo X; Zhao WY; Jiang J; Zhang CX; Gao M; Chen XF; Dong YZ Biodegradable amino-ester nanomaterials for Cas9 mRNA delivery *in vitro* and *in vivo*. *ACS Appl. Mater. Interfaces* 2017, 9, 25481–25487. [PubMed: 28685575]
- [20]. Stephen ZR; Kievit FM; Zhang MQ Magnetite nanoparticles for medical MR imaging. *Mater. Today* 2011, 14, 330–338.
- [21]. Szpak A; Fiejdasz S; Prendota W; Strazek T; Kapusta C; Szmyd J; Nowakowska M; Zapotoczny S T1–T2 dual-modal MRI contrast agents based on superparamagnetic iron oxide nanoparticles with surface attached gadolinium complexes. *J. Nanopart. Res* 2014, 16, 2678. [PubMed: 25328426]
- [22]. Li L; Jiang W; Luo K; Song HM; Lan F; Wu Y; Gu ZW Superparamagnetic iron oxide nanoparticles as MRI contrast agents for non-invasive stem cell labeling and tracking. *Theranostics* 2013, 3, 595–615. [PubMed: 23946825]
- [23]. Gossuin Y; Gillis P; Hocq A; Vuong QL; Roch A Magnetic resonance relaxation properties of superparamagnetic particles. *Wiley Interdiscip. Rev. Nanomed. Nanobiotechnol* 2009, 1, 299–310. [PubMed: 20049798]
- [24]. Weissleder R; Stark DD; Engelstad BL; Bacon BR; Compton CC; White DL; Jacobs P; Lewis J Superparamagnetic iron oxide: Pharmacokinetics and toxicity. *AJR Am. J. Roentgenol* 1989, 152, 167–173. [PubMed: 2783272]
- [25]. Zhang R; Li Y; Hu BB; Lu ZG; Zhang JC; Zhang X Traceable nanoparticle delivery of small interfering RNA and retinoic acid with temporally release ability to control neural stem cell differentiation for alzheimer's disease therapy. *Adv. Mater* 2016, 28, 6345–6352. [PubMed: 27168033]
- [26]. Chen YC; Min CN; Wu HC; Lin CT; Hsieh WY *In vitro* evaluation of the L-peptide modified magnetic lipid nanoparticles as targeted magnetic resonance imaging contrast agent for the nasopharyngeal cancer. *J. Biomater. Appl* 2013, 28, 580–594. [PubMed: 23174955]
- [27]. Albuquerque J; Moura CC; Sarmento B; Reis S Solid lipid nanoparticles: A potential multifunctional approach towards rheumatoid arthritis theranostics. *Molecules* 2015, 20, 11103–11118. [PubMed: 26087258]
- [28]. Oumzil K; Ramin MA; Lorenzato C; Hémadou A; Laroche J; Jacobin-Valat MJ; Mornet S; Roy CE; Kauss T; Gaudin K et al. Solid lipid nanoparticles for image-guided therapy of atherosclerosis. *Bioconjug. Chem* 2016, 27, 569–575. [PubMed: 26751997]
- [29]. Bai J; Wang JTW; Rubio N; Protti A; Heidari H; Elgogary R; Southern P; Al-Jamal WT; Sosabowski J; Shah AM et al. Triple-modal imaging of magneticallytargeted nanocapsules in solid tumours *in vivo*. *Theranostics* 2016, 6, 342–356. [PubMed: 26909110]
- [30]. Guo RM; Cao N; Zhang F; Wang YR; Wen XH; Shen J; Shuai XT Controllable labelling of stem cells with a novel superparamagnetic iron oxide-loaded cationic nanovesicle for MR imaging. *Eur. Radiol* 2012, 22, 2328–2337. [PubMed: 22653284]
- [31]. Sharma VK; Alipour A; Soran-Erdem Z; Aykut ZG; Demir HV Highly monodisperse low-magnetization magnetite nanocubes as simultaneous T1-T2 MRI contrast agents. *Nanoscale* 2015, 7, 10519–10526. [PubMed: 26010145]

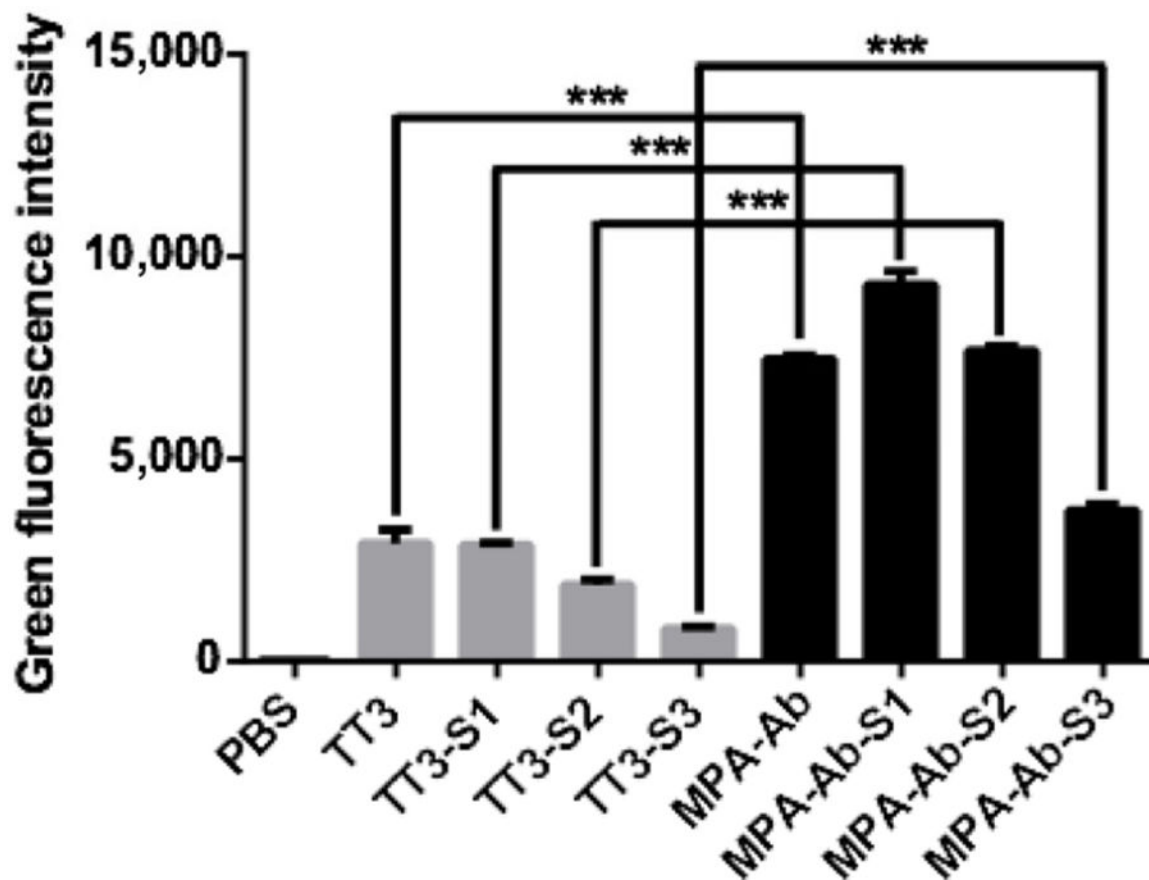


**Figure 1.** MPA-Ab LLN- and TT3 LLN-mediated eGFP expression in Hep3B cells. MPA-Ab LLNs demonstrated significantly higher eGFP mRNA delivery efficiency than TT3 LLNs with the same amount of SPIONs. \*\* $P < 0.01$ ; \*\*\* $P < 0.001$ , two-tailed  $t$ -test, triplicate measurements.

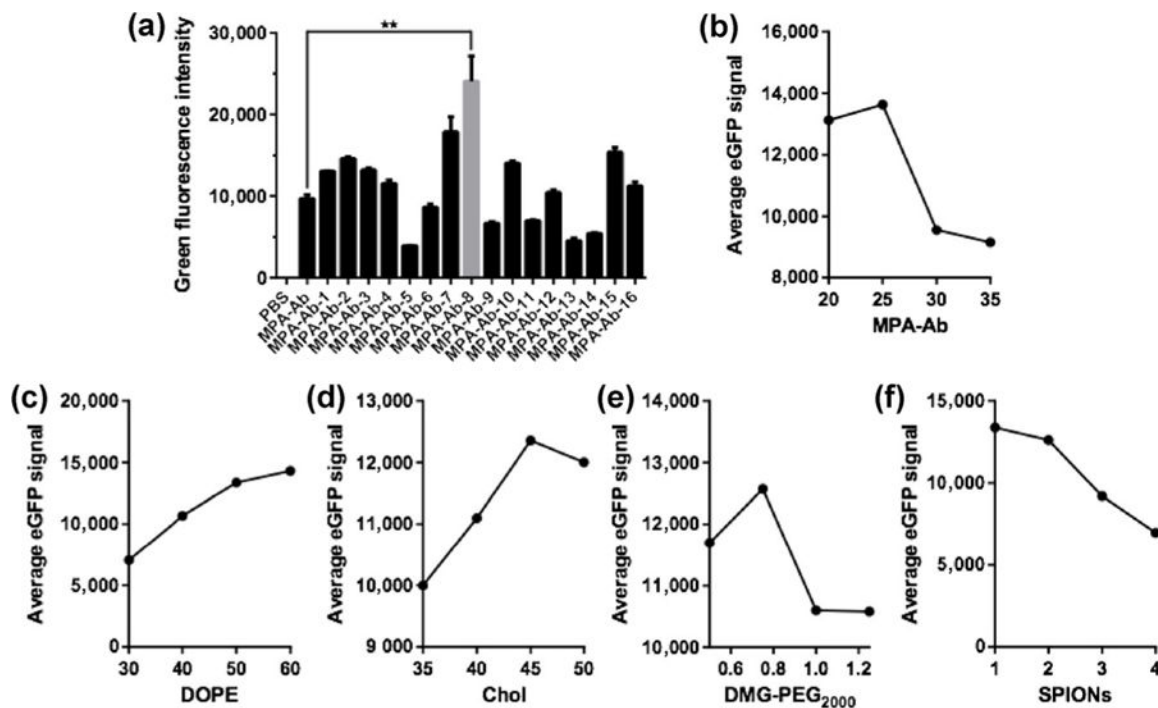


**Figure 2.**

Orthogonal experiment and trend analysis. (a) eGFP expression of 16 formulations was evaluated in Hep3B cells using an orthogonal design. The original formulation MPA-Ab was included as a control. (b)–(f) Impact trend of each factor on eGFP expression.  $**P < 0.01$ ; two-tailed *t*-test, triplicate measurements.

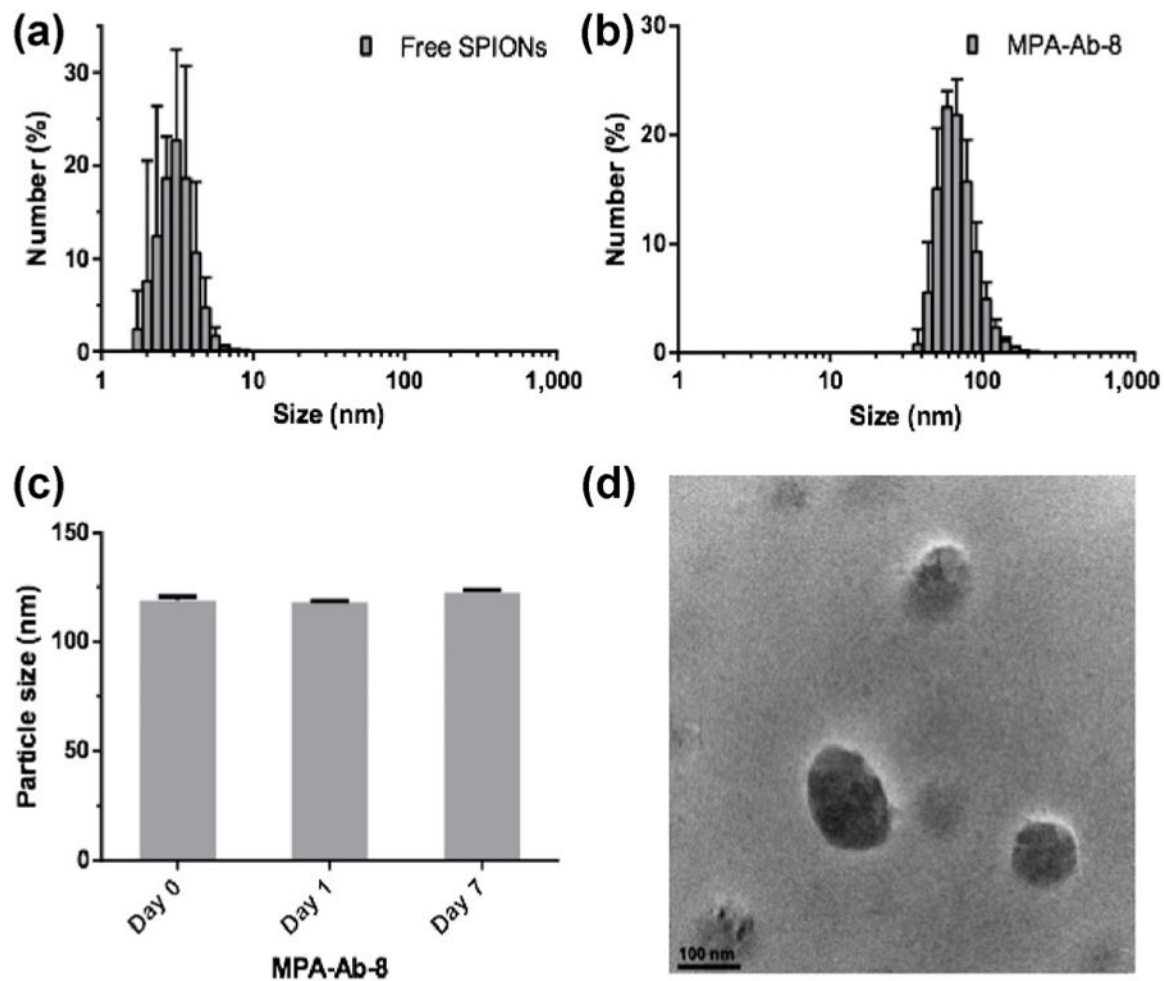


**Figure 3.** Characterization of MPA-Ab-8 LLNs. (a) Particle size distribution of free SPIONs. (b) Particle size distribution of MPA-Ab-8 LLNs. (c) Stability test of MPA-Ab-8 LLNs. (d) A representative cryoTEM image of MPA-Ab-8 LLNs. Scale bar: 100 nm.

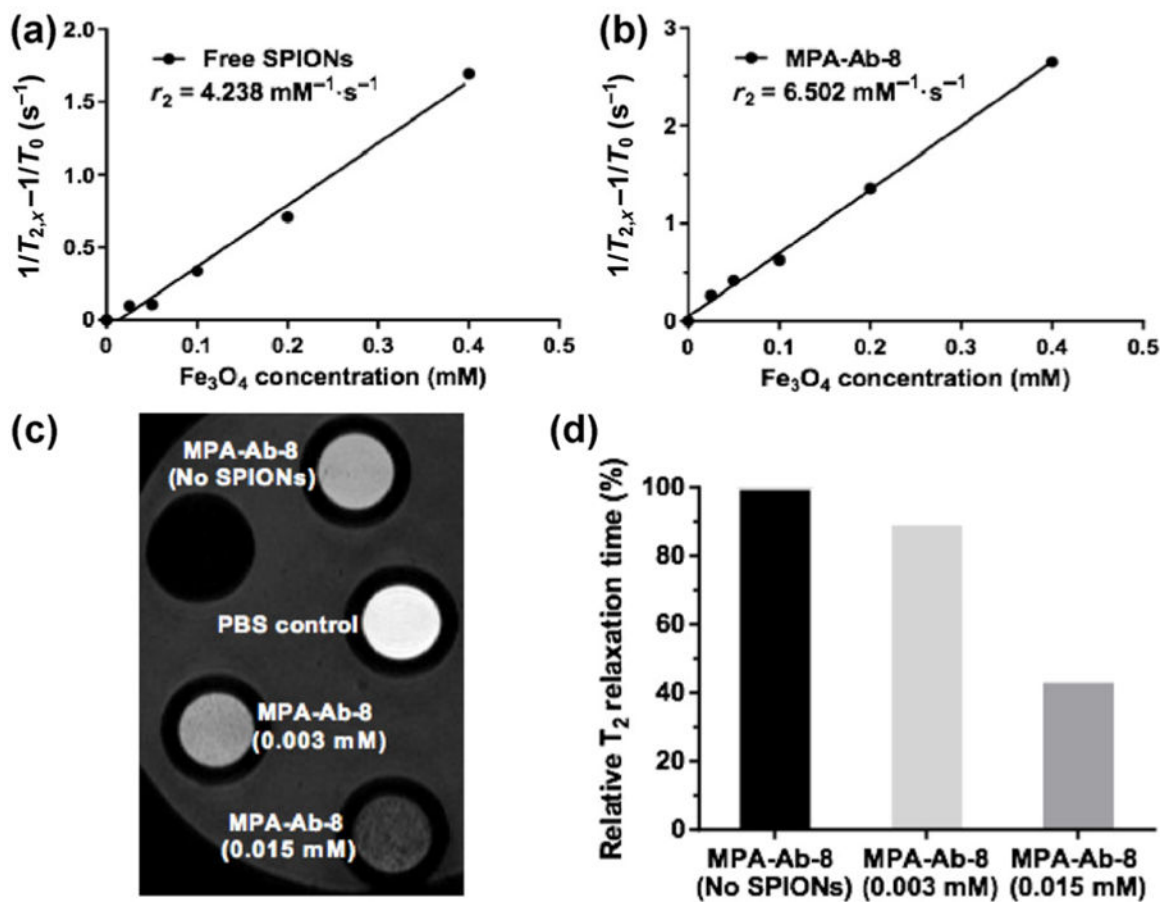


**Figure 4.** Phantom and *in-vitro* cell pellet MRI studies. (a)  $r_2$  relaxivity plot of free SPIONs determined at 9.4 T. (b)  $r_2$  relaxivity plot of formulation MPA-Ab-8 determined at 9.4 T. (c)  $T_2$ -weighted image of cell pellets. (d) Relative  $T_2$  relaxation time of cell pellets after normalization to the control.

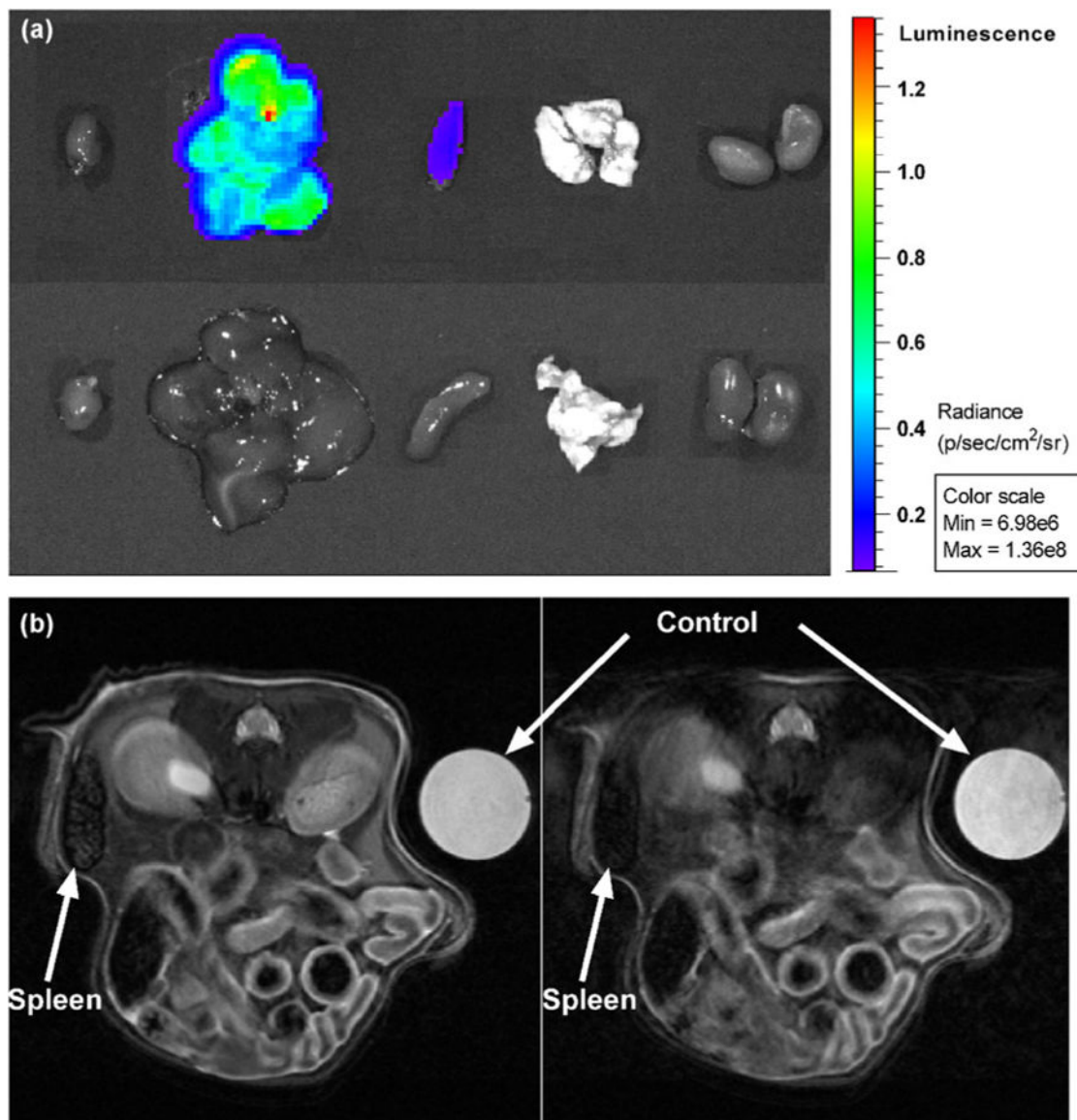


**Figure 5.** *In-vivo* biodistribution and MRI study of formulation MPA-Ab-8 ( $n = 1$ ). (a) Luminescence intensity in five organs: heart, liver, spleen, lung, and kidney (from left to right). Top: MPA-Ab-8 FLuc LLN-treated mouse. Bottom: non-treated control mouse. (b) Representative T<sub>2</sub>-weighted images of spleen. Left: before treatment. Right: immediately after treatment. Control: 1% agarose.